Photonics **2015**, *2*, 594-603; doi:10.3390/photonics2020594

OPEN ACCESS

photonics

ISSN 2304-6732

www.mdpi.com/journal/photonics

Article

Plasmonic Terahertz Amplification in Graphene-Based Asymmetric Hyperbolic Metamaterial

Igor Nefedov [1,*] and Leonid Melnikov [2]

[1] School of Electrical Engineering, Aalto University, P.O. Box 13000, Aalto 00076, Finland

[2] Yuri Gagarin State Technical University of Saratov, 77, Politekhnicheskaya, Saratov 410054, Russia; E-Mail: lam-pels@yandex.ru

* Author to whom correspondence should be addressed; E-Mail: igor.nefedov@aalto.fi; Tel.: +358-442-709-251.

Received: 21 April 2015 / Accepted: 18 May 2015 / Published: 27 May 2015

Abstract: We propose and theoretically explore terahertz amplification, based on stimulated generation of plasmons in graphene asymmetric hyperbolic metamaterials (AHMM), strongly coupled to terahertz radiation. In contrast to the terahertz amplification in resonant nanocavities, AHMM provides a wide-band THz amplification without any reflection in optically thin graphene multilayers.

Keywords: terahertz amplification; graphene multilayer; asymmetric hyperbolic metamaterials

PACS classifications: 44.40.+a; 41.20.Jb; 42.25.Bs; 78.67.Wj

1. Introduction

Nowadays, carbon-based nanomaterials are considered as attractive candidates for the development of next generation photonic devices. Generation of terahertz (THz) radiation by optically excited aligned carbon nanotubes, and single layer graphene was reported in [1–3]. These mainly experimental works demonstrate a practical possibility to obtain THz emission from carbon nanostructures. However, theoretical background of physical mechanisms, responsible for the THz emission, is practically absent in these papers. Recently it was shown, that at sufficiently strong optical pumping the real part of

dynamic conductivity of graphene becomes negative in the terahertz (THz) range due to the interband population inversion that results in amplification of the THz plasmons [4]. In order to provide a coupling of THz radiation with graphene it was proposed to use an array of resonant nanocavities in form of a periodic graphene strip line [5–8]. The disadvantage of this approach is its resonant nature that results in a narrow-band amplification (this does not relate to lasing). Besides, an amplified THz radiation is distributed between the reflected and transmitted waves. In this paper, we suggest an alternative approach for realization of the THz amplification in graphene-based plasmonic periodic structures, which exhibit properties of hyperbolic metamaterials (HMM) under certain conditions [9]. Hyperbolic metamaterials [10] are uniaxial dielectric composites, characterized with two permittivity tensor components: transverse $\epsilon_\perp$ and axial $\epsilon_\parallel$, such that $\mathrm{Re}(\epsilon_\perp)\mathrm{Re}(\epsilon_\parallel) < 0$, $\mathrm{Re}(\epsilon_{\perp,\parallel}) >> \mathrm{Im}(\epsilon_{\perp,\parallel})$. Hyperbolic metamaterials are characterized with unclosed (hyperbolic-type) surface of dispersion in space of wave vectors that manifests an ability of HMMs to support propagation of waves with very large wave vector components in certain directions. From a physical point of view it means a very high electromagnetic density of states (DOS) that appears as a high rate of spontaneous emission [11] and enhancement of all processes of light-matter interaction.

However, high DOS photons in HMMs are not coupled with photons in vacuum due to the total internal reflection. In order to overcome this problem, recently we suggested a new concept of applications of HMMs, referred as *asymmetric hyperbolic metamaterials (AHMMs)* [12]. Asymmetric hyperbolic metamaterial is a hyperbolic metamaterial with an optical axis, tilted with respect to a medium interface. Its schematic view is shown in Figure 1, where the employed Cartesian coordinate systems (x, y, z) and (x', y', z') are defined. Asymmetry appears as a difference in properties of waves, propagating upward and downward with respect to the metamaterial interface under a fixed transverse wave vector component. The most important feature of AHMM is a possibility to excite a very slow wave in AHMM by a plane wave, incoming from free space, while a minimal reflection may be achieved [13]. By other words, high density of states photons, excited in AHMM, can be perfectly coupled with photons in free space. Particularly, for graphene-based AHMM, this results in a broad-band total absorption of radiation in optically ultrathin layers of AHMM [14] or in a strong gain in a thin layer of active graphene-based AHMM, as will be demonstrated in this paper. Finally, we note that our consideration relates to the TM-polarized waves, so the p-polarized component of radiation only is amplified.

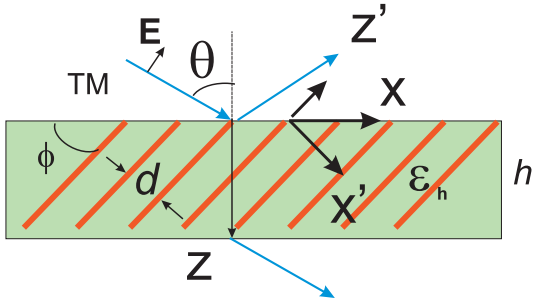

Figure 1. A sketch of amplifying graphene-based asymmetric hyperbolic metamaterial. Graphene sheets are orthogonal to the $(x'z')$-plane and periodically arranged in the x'-direction. h denotes the thickness of graphene multilayer.

2. Dynamic Conductivity of Graphene with Inversed Population of Carriers and the Effective Permittivity of the Graphene-Based AHMM

The model of the surface conductivity of graphene under pumping by optical illumination or by injection of electrons and holes was suggested in [4]. Electron and hole densities in graphene can substantially exceed their equilibrium values and the electron and hole systems can be characterized by the quasi-Fermi energies $\pm\mathcal{E}_F$, respectively, and the effective temperature T. The response of pumped graphene can be described by its complex-valued surface conductivity in the local approximation [4]

$$\sigma(\omega) = \left(\frac{e^2}{4\hbar}\right)\left\{\frac{8k_BT\tau}{\pi\hbar(1-i\omega\tau)}\ln\left[1+\exp\left(\frac{\mathcal{E}_F}{k_BT}\right)\right]+ \right.$$
$$\left. +\tanh\left(\frac{\hbar\omega-2\mathcal{E}_F}{4k_BT}\right)-\frac{4\hbar\omega}{i\pi}\int_0^\infty\frac{G(\mathcal{E},\mathcal{E}_F)-G(\hbar\omega/2,\mathcal{E}_F)}{(\hbar\omega)^2-4\mathcal{E}^2}d\mathcal{E}\right\} \quad (1)$$

Here ω is the frequency of the incident THz wave, e is the electron charge, $\hbar$ is the reduced Planck constant, k_B is the Boltzmann constant, T is the temperature, τ is the phenomenological electron and hole scattering time, and

$$G(\mathcal{E},\mathcal{E}') = \frac{\sinh(\mathcal{E}/k_BT)}{\cosh(\mathcal{E}/k_BT)+\cosh(\mathcal{E}'/k_BT)} \quad (2)$$

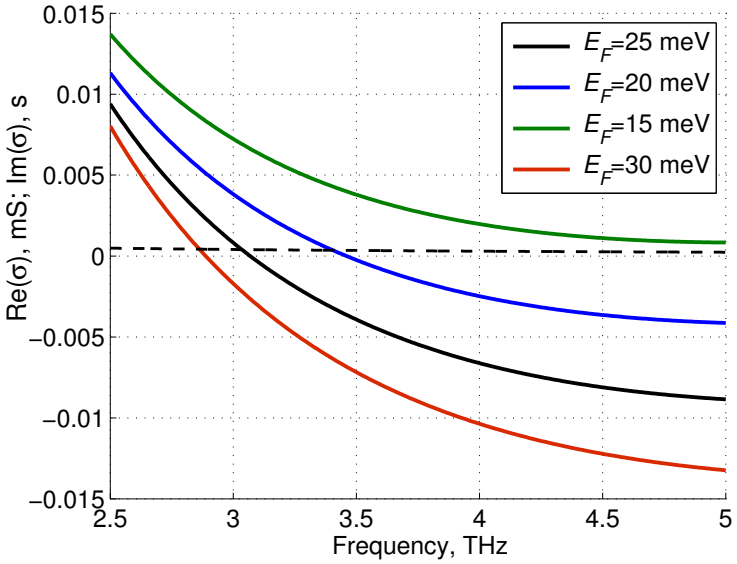

Figure 2. Real part of the dynamic conductivity, calculated for different $\mathcal{E}_F$ Imaginary part of σ calculated at $\mathcal{E}_F$ = 25 meV, is shown by the dashed curve.

Figure 2 shows that the real part of the dynamic graphene conductivity changes sign at terahertz frequencies and graphene becomes an active material. At the same time, the imaginary part of the conductivity is positive, (≈ 0.3 mS), *i.e.*, graphene can be considered as an inductive impedance surface.

Let us consider a graphene multilayer, formed of periodically arranged graphene sheets with period d, embedded into a host matrix. Dispersive properties of such a graphene metamaterial have been studied in [9], where the periodicity was taken into account. Here, we use the effective medium model which was

verified comparing with the more accurate model (see [14]). The effective relative permittivity tensor of the graphene multilayer (Maxwell-Garnett homogenization) has form:

$$\bar{\bar{\epsilon}} = \begin{bmatrix} \epsilon_{\|} & 0 & 0 \\ 0 & \epsilon_{\perp} & 0 \\ 0 & 0 & \epsilon_{\perp} \end{bmatrix} \tag{3}$$

Two diagonal components of the relative permittivity tensor in the coordinate system (x', y', z') read as $\epsilon_{\|} = \epsilon_{x'x'} = \epsilon_h$,

$$\epsilon_{\perp} = \epsilon_{y'y'} = \epsilon_{z'z'} = \epsilon_h + i\frac{\sigma}{d\omega\epsilon_0} \tag{4}$$

where ϵ_h is the permittivity of a host matrix, ϵ_0 is the permittivity of vacuum. Figure 3 illustrates the frequency dependence of $\epsilon_{\perp}$ for the graphene-based AHMM, described in terms of the effective medium theory. One can see that $\mathrm{Im}(\epsilon_{\perp})$ changes sign at the frequency 3.08 THz. At the same time, $\mathrm{Re}(\epsilon_{\perp})$ is the negative up to ≈ 4 THz.

The host matrix also may be inhomogeneous with period consisting of two or more layers (substrates for graphene sheets). In this case the structure can be considered as a photonic hypercrystal [15] and we can speak about an effective permittivity of the host matrix. Thus, choosing period d and the effective anisotropic permittivity ϵ_h we can engineer an active HMM for a required frequency range.

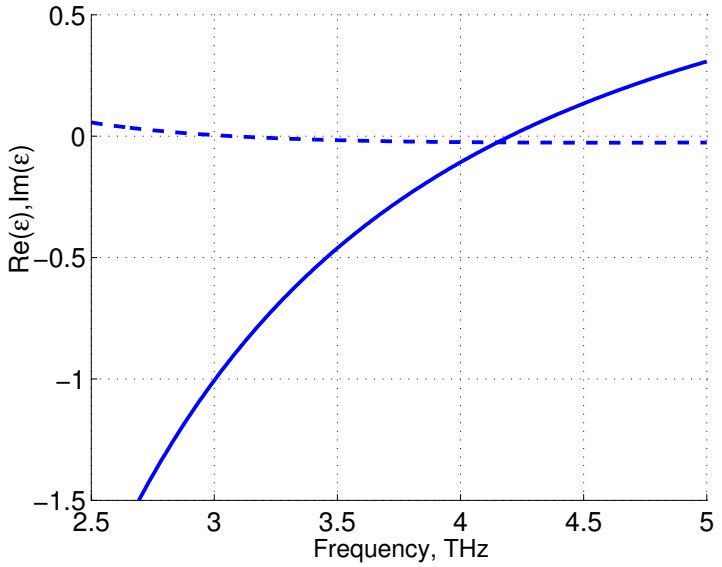

Figure 3. $\epsilon_{\perp}$ of the graphene multilayer, calculated at $\epsilon_h = 1.01$, $d = 1.2\,\mu$m, $\mathcal{E}_F = 28$ meV, $\tau = 10^{-12}$ s, $T = 300$ K. Solid and dashed curves correspond to the real and imaginary parts of $\epsilon_{\perp}$, respectively.

3. Eigenwaves and Energy Flows in AHMM

To solve the problem of electromagnetic wave transmission through a slab of AHMM we have to find normal wave vector components k_z in coordinate system (xyz), associated with slab interfaces. First we transform the permittivity tensor components to the system (xyz), where it takes a non-diagonal form.

As stated above, the permittivity tensor of the graphene metamaterial has the Equation (3) in the primed coordinate system $x', y', z')$. The Cartesian components of $\bar{\bar{\epsilon}}$ in the coordinate system (x, y, z) read:

$$\begin{aligned} \epsilon_{xz} &= \epsilon_{zx} = (\epsilon_{\parallel} - \epsilon_{\perp}) \cos\phi \sin\phi \\ \epsilon_{xx} &= \epsilon_{\perp} \sin^2\phi + \epsilon_{\parallel} \cos^2\phi \\ \epsilon_{zz} &= \epsilon_{\perp} \cos^2\phi + \epsilon_{\parallel} \sin^2\phi \end{aligned} \tag{5}$$

Thus, the permittivity tensor becomes non-diagonal, but symmetric, *i.e.*, $\epsilon_{xz} = \epsilon_{zx}$. Substituting the tensor components Equation (5) into Maxwell equations, we obtain the normal component of the wave vector in AHMM [13]:

$$k_z^{(1,2)} = \frac{-k_x \epsilon_{xz} \pm \sqrt{(\epsilon_{xz}^2 - \epsilon_{xx}\epsilon_{zz})(k_x^2 - k_0^2 \epsilon_{zz})}}{\epsilon_{zz}} \tag{6}$$

where $k_x = k_0 \sin\theta$ and $k_0 = \omega/c$, is determined by the incidence angle θ. Here $k_z^{(1)}$, $k_z^{(2)}$, correspond to signs "+" and "−", respectively.

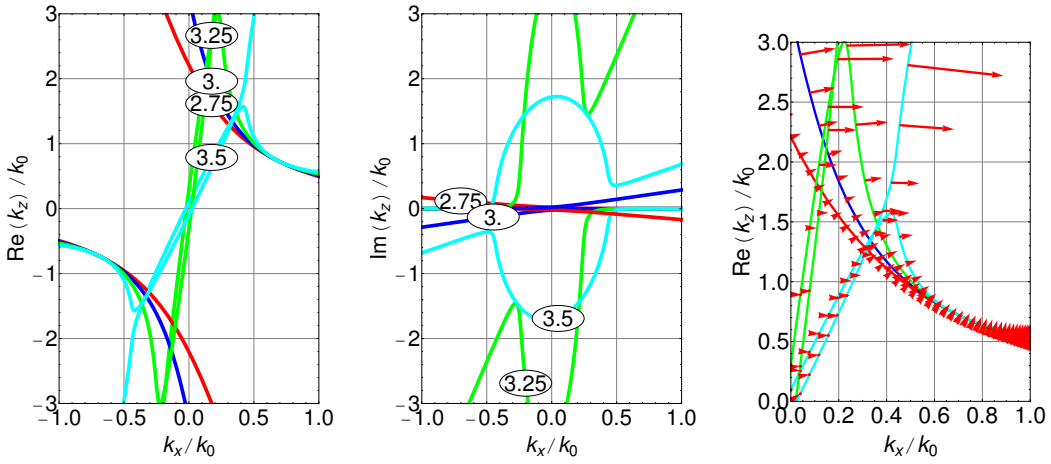

Figure 4. Isofrequencies of the graphene multilayer medium (real part of k_z (**a**), imaginary part of k_z (**b**)), calculated for frequencies 2.75 (red), 3 (blue), 3.25 (green), and 3.5 (cyan) THz and energy flow directions (c), calculated for the same set of parameters as in Figure 3 and $\phi = 44°$.

In Figure 4 the isofrequencies $\omega(k_z, k_x) = const = 2.75 \ldots 3.5$ THz are shown $(k_y = 0)$. Since k_z is complex for gain or loss medium, providing the frequency ω is real, the isofrequencies at the planes $k_x/k_0, \mathrm{Re}(k_z)/k_0$ and $k_x/k_0, \mathrm{Im}(k_z)/k_0$ are shown separately, demonstrating hyperbolic dispersion (Figure 4a), gain for the frequencies 3.0, 3.25, and 3.5 THz and losses for 2.75 THz (Figure 4b). The directions of energy flow were calculated using the components of Pointing vector: $\vec{S} = (1/2)\mathrm{Re}(\vec{E}^* \times \vec{H}) = \{S_x, 0, S_z\}$, where the medium eigenwaves vectors are $\vec{H} = \{0, H_y, 0\}$, $H_y \propto k_x \sin\phi - k_z \cos\phi$, $\vec{E} \propto -\bar{\bar{\epsilon}}^{-1}(\vec{k} \times \vec{H})$. In Figure 4c the red arrows, presenting the $\vec{S}$, are plotted along the corresponding isofrequency curves demonstrating the directions of energy flow. Due to different scales along k_x and k_z axes the directions of $\vec{S}$ were changed $\{S_x, S_z\} \to \{S_x, 3S_z\}$ to show visually the orthogonality of the directions of energy flow to the isofrequencies in the regions of waves propagating

with low losses/gain. These results are useful for choosing the proper branches of the solutions for k_z, and demonstrate that the energy flows go mostly along the x-axis of the multilayer.

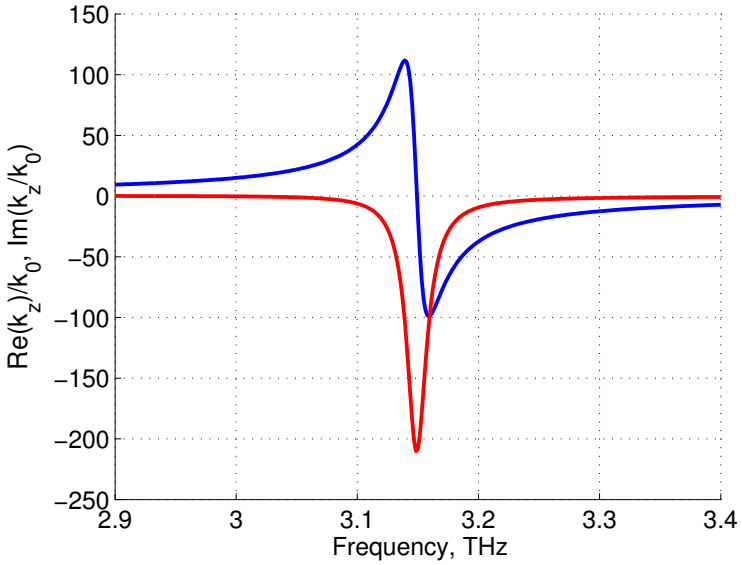

Figure 5. Real (blue) and imaginary (red) parts of $k_z^{(2)}/k_0$, calculated at $\mathcal{E}_F = 28$ meV, $\varphi = 44°$, $k_x = k_0 \sin\theta$, $\theta = 44°$, $\epsilon_h = 1.01$, $d = 1.2\,\mu$m, $\tau = 10^{-12}$ s, $T = 300$ K.

Figure 5 demonstrates the Lorentz resonance-like dependence of $k_z^{(2)}$. It shows that in vicinity of the frequency $f_0 \approx 3.1$ THz the real part of $k_z^{(2)}/k_0$ changes sign and becomes very large. At the same time, $\mathrm{Im}(k_z^{(2)})/k_0$ is very large and negative that demonstrates a gain in AHMM. The value of $k_z^{(1)}$ is small, approximately the same as in host medium, since it corresponds to the wave whose electric field vector is orthogonal to graphene sheets and does not interact with the graphene plasmonic system. Note that this resonance is not a size resonance since the size does not enter Equation (6) and the resonant frequency depends only on such a geometrical parameter as the tilt angle ϕ. We will show below that despite $\mathrm{Re}(k_z^{(2)})/k_0$ and $\mathrm{Im}(k_z^{(2)})/k_0$ are very large, the perfect matching with free space can be achieved [13,14] and the most efficient interaction between an incoming radiation and plasmonic system can be provided.

4. Amplification of Terahertz Radiation

Next, we will consider a plane wave propagation through a finite-thickness slab of the graphene-based AHMM using the 2×2 transfer matrix method, modified for the general case $k_z^{(1)}(k_x) \neq k_z^{(2)}(k_x)$. This transfer matrix reads [13]:

$$\overline{\overline{M}} = \begin{bmatrix} M_{11} & M_{12} \\ M_{21} & M_{22} \end{bmatrix} = \begin{bmatrix} \frac{Z_1 e^{ik_z^{(1)}W} - Z_2 e^{ik_z^{(2)}W}}{Z_1 - Z_2} & -Z_1 Z_2 \frac{e^{ik_z^{(1)}W} - e^{ik_z^{(2)}W}}{Z_1 - Z_2} \\ \frac{e^{ik_z^{(1)}W} - e^{ik_z^{(2)}W}}{Z_1 - Z_2} & \frac{Z_2 e^{ik_z^{(1)}W} - Z_1 e^{ik_z^{(2)}W}}{Z_2 - Z_1} \end{bmatrix} \tag{7}$$

where Z_1 and Z_2 are transverse wave impedances for AHMM, corresponding to upward and downward waves, which are expressed as [13]:

$$Z_{1,2} = \frac{-E_x}{H_y} = \frac{\eta_0}{k_0} \frac{\sqrt{k_x^2 - k_0^2 \epsilon_{zz}}}{\sqrt{\epsilon_{xz}^2 - \epsilon_{xx}\epsilon_{zz}}} \tag{8}$$

where $\eta_0 = 120\pi\,\Omega$. For low-loss HMM with Im($\epsilon_\parallel$)=0, $\epsilon_\perp = \alpha + i\delta$, $\delta << \alpha$, the Brewster angle θ_B, which corresponds to zero reflection, is expressed as [16]

$$\theta_B = \arcsin\left(\sqrt{\frac{\alpha}{1+\alpha}}\right) \tag{9}$$

where $\arcsin(w) \in \left[-\frac{\pi}{2}, \frac{\pi}{2}\right]$.

The transmission coefficient t can be calculated using the formula:

$$t = \frac{2}{M_{11} + M_{22} + M_{12}/Z_0 + M_{21}Z_0} \tag{10}$$

where $Z_0 = \eta\sqrt{k_0^2 - k_x^2}/k_0$. The reflection coefficient reads as

$$R = \frac{M_{11} + M_{12}/Z_0 - M_{21}Z_0 - M_{22}}{M_{11} + M_{22} + M_{12}/Z_0 + M_{21}Z_0} \tag{11}$$

Absorption A is defined as

$$A = 1 - |R|^2 - |t|^2 \tag{12}$$

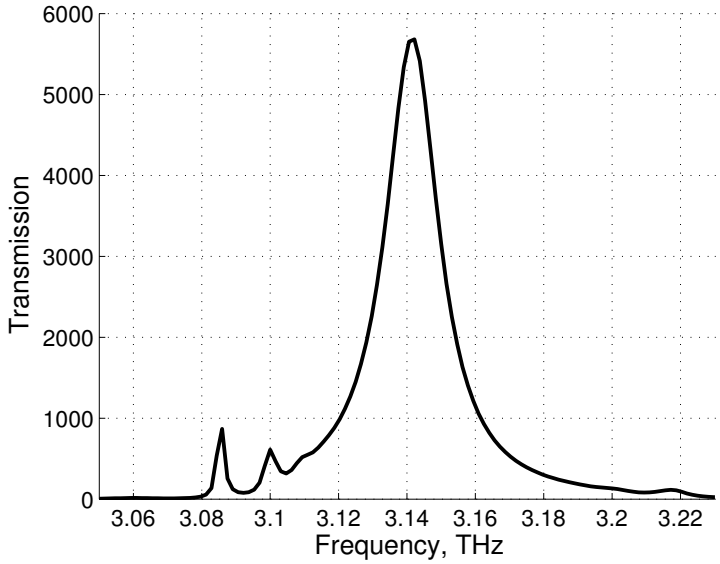

Figure 6. Amplified transmission, calculated at the same asymmetric hyperbolic metamaterials (AHMM) parameters as above. The thickness of the graphene-based AHMM slab $h = 10\,\mu$m.

Figure 6 illustrates transmission of the plane THz wave trough the graphene-based amplifying structure. Note, that the reflection is practically absent. Here we observe a wider amplification band, 0.6% instead 0.03%, estimated from [5] at the same $\tau = 10^{-12}$ s. The peak of transmission corresponds to the plasmon lasing regime which correct consideration demands nonlinear theory of graphene conductivity in the field of THz radiation. We expect, that the limitations of our model is similar to claimed in [5], that is about 10^3.

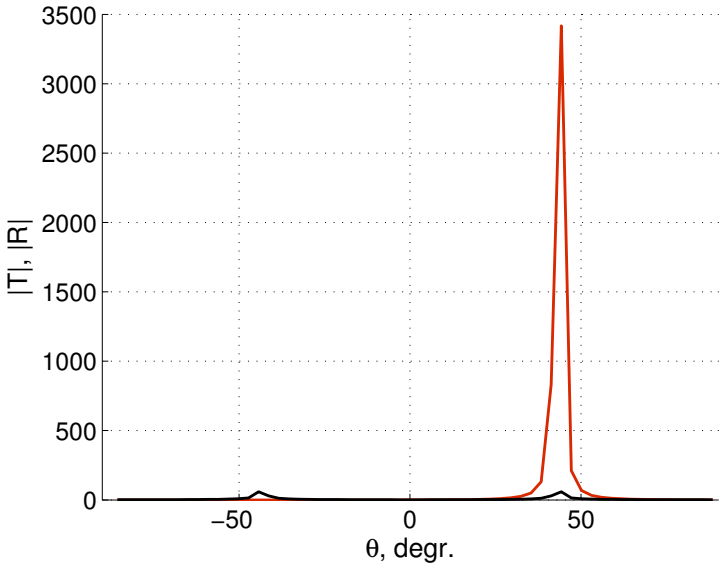

Figure 7. Transmission (red) and reflection (black) coefficients.

The angle dependence of amplification, calculated at 3.14 THz, and the same as above other parameters, is shown in Figure 7. Here we observe amplification not only for the transmitted wave, but also for the reflected one. However, the peak of amplified reflected wave is about of 60 that 60 times less than the height of the transmission peak. Figure 7 demonstrates a high sensitivity of amplification to the incidence angle θ. The angle asymmetry appears only for the transmission.

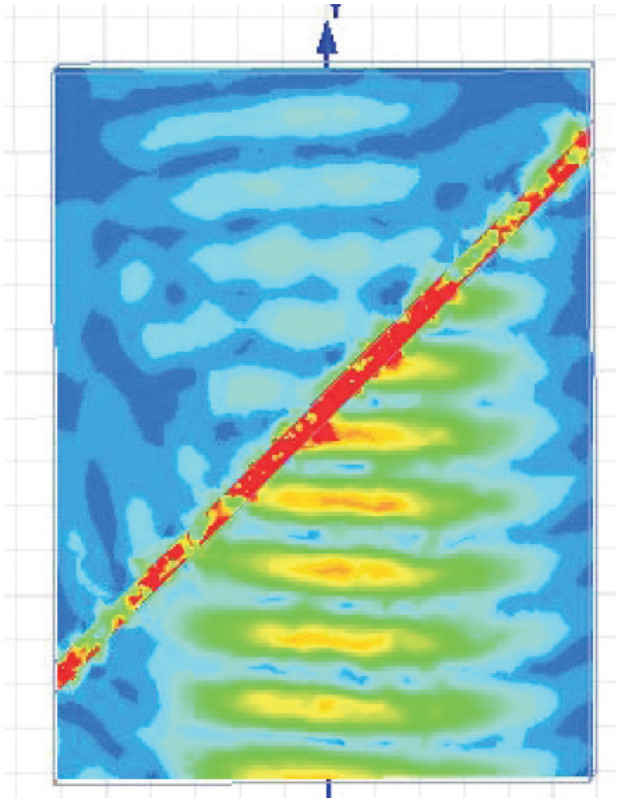

Figure 8. Amplification of the Gaussian beam, shown in the x', z' plane.

Figure 8 shows result of ANSOFT HFSS numerical simulation for a Gaussian beam, incident onto graphene-based amplifying AHMM. The optical axis is parallel to the z'-axis, as in Figure 1. Narrow Gaussian beam and absorbing boundary conditions were used due to the absence of the (x, y) symmetry plane for this structure. Simulations were implemented at the frequency $f = 3.14\,\text{THz}$. The slab thickness equals to $\lambda/10$, where λ is the wavelength of the incident light.

5. Conclusions

In conclusions, we have suggested a structure, potentially realizing extremely strong coupling between photons in free space and high density of states THz plasmons, excited in graphene-based AHMM. A giant amplification of terahertz radiation in this structure can be achieved due to the stimulated generation of plasmons in graphene sheets. Unlike amplification of surface plasmons in an array of graphene resonant nanocavities [5], plasmons in AHMM can be considered as "volume plasmons" in the metamaterial. Due to the absence of such resonant elements as micro/nanocavities, we obtain a significantly wider-band amplification. Existence of the lasing regime also is observed, however, its investigation cannot be implemented in framework of a linear model. Despite of technological difficulties associated with the manufacture of asymmetric graphene-based HMM, we consider our approach as a promising for creation of plasmonic graphene amplifiers and generators for the THz frequency range. Asymmetric HMMs can be fabricated from any plasmonic materials, such as metallic carbon nanotubes [13], noble metals [12,17] and doped silicon [12], *etc.* Since in this work the considered metamaterial is the periodic structure with a very small period, much smaller than a THz wavelength and considerably smaller, than the wavelength in AHMM, we could exploit the local effective medium model. More accurate nonlocal models, like [18], which take into account a spatial dispersion, may be used if needed.

Author Contributions

I.N. initiated the study, L.M. and I.N. conducted the analytical analysis, L.M. conducted the calculations of isofrequencies and velocities, I.N. conducted the calculations of gain, reflection/transmission, and ANSOFT HFSS numerical calculations, I.N. and L.M. wrote the manuscript.

Conflicts of Interest

The authors declare no conflict of interest.

References

1. Titova, L.V.; Pint, C.L.; Zhang, Q.; Hauge, R.H.; Kono, J.; Hegmann, F.A. Generation of Terahertz Radiation by Optical Excitation of Aligned Carbon Nanotubes. *Nano Lett.* **2015**, *15*, 3267–3272.
2. Bahk, Y.-M.; Ramakrishnan, G.; Choi, J.; Song, H.; Choi, G.; Kim, Y.H.; Ahn, K.J.; Kim, D.S.; Planken, P.C.M. Plasmon Enhanced Terahertz Emission from Single Layer Graphene. *ACS Nano* **2014**, *8*, 9089–9096.

3. Obraztsov, P.A.; Kanda, N.; Konishi, K.; Kuwata-Gonokami, M.; Garnov, S.V.; Obraztsov, A.N.; Svirko, Y.P. Photon-drag-induced terahertz emission from graphene. *Phys. Rev. B* **2014**, *B*, 241416(R).
4. Dubinov, A.A.; Aleshkin, V.Y.; Mitin, V.; Otsuji, T.; Ryzhii, V. Terahertz surface plasmons in optically pumped graphene sytuctures. *J. Phys. Condens. Matter.* **2011**, *23*, 145302.
5. Popov, V.V.; Polischuk, O.V.; Davoyan, A.R.; Ryzhii, V.; Otsuji, T.; Shur, M.S. Plasmonic terahertz lasing in an array of graphene nanocavities. *Phys. Rev. B* **2012**, *86*, 195437.
6. Popov, V.V.; Polischuk, O.V.; Nikitov, S.A.; Ryzhii, V.; Otsuji, T.; Shur, M.S. Amplification and lasing of terahertz radiation by plasmons in graphene with a planar distributed Bragg resonator. *J. Opt.* **2013**, *15*, 114009.
7. Otsuji, T.; Watanabe, T.; Tombet, S.A.B.; Satou, A.; Knap, W.M.; Popov, V.V.; Ryzhii, M.; Ryzhii, V. Emission and Detection of Terahertz Radiation Using Two-Dimensional Electrons in III-V Semiconductors and Graphene. *IEEE Trans. Terahertz Sci. Techn.* **2013**, *3*, 63–71.
8. Otsuji1, T.; Popov, V.; Ryzhii, V. Active graphene plasmonics for terahertz device applications. *J. Phys. D Appl. Phys.* **2014**, *47*, 094006 .
9. Iorsh, I.V.; Mukhin, I.S.; Shadrivov, I.V.; Belov, P.A.; Kivshar, Y.S. Hyperbolic metamaterials based on multilayer graphene structures. *Phys. Rev. B* **2013**, *87*, 075416.
10. Poddubny, A.; Iorsh, I.; Belov, P.; Kivshar, Y. Hyperbolic metamaterials. *Nature Photonics* **2013**, *7*, 958–967.
11. Poddubny, A.N.; Belov, P.A.; Kivshar, Y.S. Spontaneous radiation of a finite-size dipole emitter in hyperbolic media. *Phys. Rev. A* **2011**, *84*, 023807.
12. Nefedov, I.S.; Valagiannopoulos, C.A.; Hashemi, S.M.; Nefedov, E.I. Total absorption in asymmetric hyperbolic media. *Sc. Rep.* **2013**, *3*, 2662.
13. Hashemi, S.M.; Nefedov, I.S. Wideband perfect absorption in arrays of tilted carbon nanotubes. *Phys. Rev. B* **2012**, *86*, 195411.
14. Nefedov, I.S.; Valagiannopoulos, C.A.; Melnikov, L.A. Perfect absorption in graphene multilayers. *J. Opt.* **2013**, *15*, 114003.
15. Narimanov, E.E. Photonic Hypercrystal. *Phys. Rev. X* **2014**, *4*, 041014.
16. Valagiannopoulos, C.A.; Nefedov, I.S. On increasing the electromagnetic attenuation below a quasi-matched surface with use of passive hyperbolic metamaterials. *Photon. Nano. Fundament. Appl.* **2013**, *11*, 182–190.
17. Dutta, J.; Ramakrishna, S.A.; Lakhtakia, A. Asymmetric coupling and dispersion of surface-plasmon-polariton waves on a periodically patterned anisotropic metal film. *J. Appl. Phys.* **2015**, *117*, 013102.
18. Chebykin, A.V.; Orlov, A.A.; Simovski, C.R.; Kivshar, Y.S.; Belov, P.A. Nonlocal effective parameters of multilayered metal-dielectric metamaterials. *Phys. Rev. B* **2012**, *86*, 115420.